(Received 22 July 2024, Accepted 5 October 2024, Scheduled 14 October 2024)

Design of Multimode Hybrid Power Amplifier Based on Interdigital Bandpass Filter

Shiwei Zhao[1, 2, *], Linsong Li[1], Sijia Li[2], Zuqiang Zhang[3], Longfei Zhou[1], and Fei Zhao[1]

[1]*Electromagnetic Field and Wireless Technology Innovation Laboratory Chongqing University of Posts and Telecommunications, Chongqing, China*
[2]*Chongqing Jiadan Microelectronics Co., Ltd, Chongqing, China*
[3]*Sichuan Jiuzhou Electric Appliance Group Co. Ltd, Mianyang, Sichuan, China*

ABSTRACT: This paper introduces a multimode hybrid continuous class power amplifier utilizing a band-pass filter. It integrates resistive response amplifiers operating in three modes: class F, class J, and class F-1. Instead of the traditional quarter-wavelength line for harmonic control, an interdigital band-pass filter is utilized to manage harmonic impedance, enabling broadband operation, high efficiency, reduced circuit size, and improved out-of-band rejection. To demonstrate the approach, a multimode hybrid broadband high-efficiency power amplifier designed for 2 to 3.8 GHz range, achieving drain efficiency from 56.3% to 75.5%, saturated output power ranging from 39.1 to 41.2 dBm, and gain between 11.1 and 13.2 dB, is detailed and fabricated in this paper.

1. INTRODUCTION

With the development of 5G mobile communication system, there is an increasing demand for wider bandwidth and high efficiency communication system, and waveform engineering technologies are widely used in communication engineering. By controlling high harmonics, the current and voltage waveforms of the circuit are modified so that the overlap between the corresponding waveforms of the current and voltage is reduced resulting in a reduction in the DC losses of the amplifier [1–5], and high efficiency and extended bandwidth can be achieved by continuous hybrid class mode of operation.

After years of study by researchers, a variety of methods for controlling harmonics have been discovered. Among them, quarter-wavelength transmission lines are widely used in many designs due to their simplicity and high fabrication accuracy [6], but most of the designs are limited by the bandwidth and are less efficient throughout the frequency band, making it difficult to balance bandwidth and efficiency. In order to solve this problem, the filter principle can be applied to the design of power amplifiers. As an indispensable part of the RF front end, the filter and power amplifier are jointly designed to perform the function of filtering clutter and impedance transformation in the circuit, which can effectively reduce the size of the circuit and improve the efficiency. For example, in [7] an all-metal cavity filter power amplifier is designed, achieving an efficiency of 51%–67% at 2.95–3.35 GHz. In [8], a 5G broadband power amplifier with a band-pass filter response is synthesized by using a spread spectrum band-pass filter as a matching network, achieving an efficiency of 47%–60% at 2–3.8 GHz. However, the above filter power amplifier does not show good efficiency and bandwidth. In this paper, a multimode hybrid power amplifier is designed with an interfinger filter structure, and it is combined with the output matching circuit of a power amplifier. On the one hand, it adopts a gap structure, and DC cannot pass through, so it plays a blocking capacitor role, protecting the circuit from the influence of DC. On the other hand, it can not only pass the ultra-wideband signal, but also suppress the signal of a specific frequency band, can effectively control the harmonic impedance of the circuit, and can achieve a good out-of-band suppression.

For switched power amplifiers, in [9] class F and inverse class F power amplifiers were designed using a quarter-wavelength transmission line harmonic control network, achieving 64% power added efficiency (PAE) and 74% PAE at 1 GHz, respectively. In [10], two class J power amplifiers were designed using a multi-stub network and a step-impedance microstrip line network. It achieves 55-68% efficiency at 1.6–2.2 GHz and 50–69% efficiency at 0.5–1.5 GHz, respectively, and it is found that traditional single-mode power amplifiers are difficult to achieve high efficiency in a wide bandwidth. The continuous class power amplifier can solve this problem effectively [11, 12], and this method can effectively increase the bandwidth of conventional switching amplifiers. However, with the further requirement of bandwidth, it is difficult to satisfy our needs with separate continuous class modes; thus, adopting mode combination theory can satisfy our needs by combining multiple continuous class amplifiers [13], which can satisfy both the bandwidth and efficiency requirements.

2. THEORETICAL ANALYSIS

Conventional microstrip band-pass filters often use parallel-coupled filters, which are designed with low cost in mind and

* Corresponding author: Shiwei Zhao (zhaosw@cqupt.edu.cn).

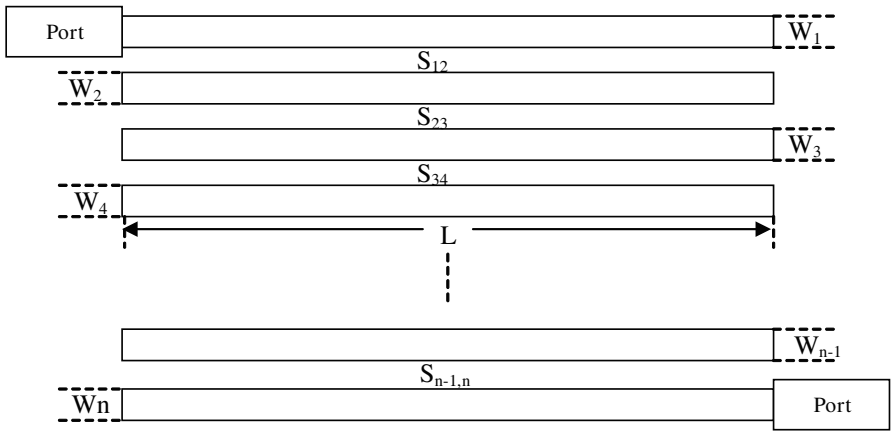

FIGURE 1. Structure of interdigital bandpass filter.

are widely used, but they exhibit spurious second harmonic responses; their size is too long; their structure is not compact enough; and they are not conducive to the integration of the system. Each resonant rod of the parallel-coupled filter is broken from the center and folded to obtain the interdigital band-pass filter. This structure is more compact; the volume is greatly reduced to facilitate the miniaturization of the system; and the gap between the coupled lines is increased, which is easy to process and manufacture and improves the consistency and reliability of the system, as shown in Fig. 1. The terminated open-circuit interdigital band-pass filter consists of two sets of rectangular-rod parallel-coupled line resonator arrays crossed over each other, each with one end of the rectangular rods short-circuited and one end open-circuited, with a wide range of relative bandwidth adaptations from a hundredth of a percent to one octave. The order n of the filter and the corresponding normalized conductance value g_i can be derived from the target parameters of the design, and the order n of the filter is derived as follows [14]:

$$n \geq \frac{\cosh^{-1}\sqrt{\dfrac{10^{0.1L_{\mathrm{As}}}}{10^{0.1L_{\mathrm{Ar}}}}-1}}{\cosh^{-1}\omega'_s} \tag{1}$$

where L_{As} represents the minimum out-of-band rejection at the normalized frequency; L_{Ar} represents the value of the passband interpolation loss fluctuating on the loss rms curve; and ω'_s represents the normalized frequency.

After determining the order of the filter and the normalized conductance value, calculate the normalized unit length self-capacitance of each rod:

$$\frac{c_1}{\varepsilon} = \frac{376.7}{\sqrt{\varepsilon_r}} Y_A \left(\frac{1-\sqrt{h}}{Z_1 Z_A}\right) \tag{2}$$

$$\frac{c_2}{\varepsilon} = \frac{376.7}{\sqrt{\varepsilon_r}} Y_A h \frac{Y_2}{Y_A} 0 - \sqrt{h}\frac{c_1}{\varepsilon} \tag{3}$$

$$\frac{c_k}{\varepsilon}|_{k=3\sim n-2} = \frac{376.7}{\sqrt{\varepsilon_r}} Y_A h \frac{Y_k}{Y_A} \tag{4}$$

$$\frac{c_{n-1}}{\varepsilon} = \frac{376.7}{\sqrt{\varepsilon_r}} Y_A h \frac{Y_{n-1}}{Y_A} - \sqrt{h}\frac{c_n}{\varepsilon} \tag{5}$$

$$\frac{c_n}{\varepsilon} = \frac{376.7}{\sqrt{\varepsilon_r}} Y_A \frac{1-\sqrt{h}}{Z_n/Z_A} \tag{6}$$

Calculate the normalized unit length mutual capacitance between two adjacent rods:

$$\frac{c_{12}}{\varepsilon} = \frac{376.7}{\sqrt{\varepsilon_r}} Y_A \frac{\sqrt{h}}{Z_1/Z_A} \tag{7}$$

$$\frac{c_{k,k+1}}{\varepsilon}|_{k=2\sim n-2} = \frac{376.7}{\sqrt{\varepsilon_r}} Y_A h \frac{J_{k,k+1}}{Y_A} \tag{8}$$

$$\frac{c_{n-1,n}}{\varepsilon} = \frac{376.7}{\sqrt{\varepsilon_r}} Y_A \frac{\sqrt{h}}{Z_n/Z_A} \tag{9}$$

where ε_r is the relative dielectric constant; Y_A is the characteristic admittance, generally 0.02; and h is the dimensionless factor obtained by Equation (10):

$$\frac{2c_{k-1,k}}{\varepsilon} + \frac{c_k}{\varepsilon} + \frac{2c_{k,k+1}}{\varepsilon} = 5.4 \tag{10}$$

Calculate the gap between adjacent guide bands:

$$S_{i-1,i}|_{i=1,2\ldots n+1} = \frac{B}{\pi}\frac{K_{i-1,i}+1}{K_{i-1,i}-1} \tag{11}$$

where $K_{i-1,i} = \exp(\frac{C_{i,i+1}}{\varepsilon K_1})$, B is the thickness of the substrate, and t is the thickness of the conductor.

Calculate the rectangle bar width:

$$\frac{W_i}{b} = \frac{1-t/b}{2}\left(\frac{c_i}{2\varepsilon} - \frac{c_{fe_i}}{\varepsilon} - \frac{c_{fe_{i+1}}}{\varepsilon}\right) \tag{12}$$

$$L = \frac{c}{4f_0\sqrt{\varepsilon_{r1}}} \tag{13}$$

where $\frac{c_{fe}}{\varepsilon} = \frac{c_f ln(1+\tanh(\theta_i))}{\pi(1-t/B)ln2}$, $\theta_i = \frac{\pi s_{i-1,i}}{2B}$. The length of the branches is obtained from formula (13) [15–17].

Traditional continuous class power amplifiers employ a technique that involves multiplying the voltage output of high-efficiency amplifiers by a reactance factor, given by $(1-\gamma\sin\theta)$. This approach effectively confines the second harmonic impedance to a purely reactive domain, forming a reactance circle. Nevertheless, achieving a precise match between the second harmonic and a purely imaginary impedance component within a wide frequency band poses a significant challenge. Based on their investigations, Carrubba and colleagues suggested enhancing the reactance factorization by integrating an impedance factor $(1+\delta\cos\theta)$ for regulating the real component of the second harmonic [18]. Class J power amplifiers are derived from class B power amplifiers, and the voltage equation for this resistive response class J power amplifier is shown in Equation (14).

$$V_{DS,RRJ}(\theta) = V_{DD}(1-\cos\theta)(1-\gamma\sin\theta)(1+\delta\cos\theta) \quad (14)$$

$$i_{D,B}(\theta) = I_{\text{Max}}\left(\frac{1}{\pi}+\frac{1}{2}\cos\theta+\frac{2\pi}{3}\cos 2\theta-\frac{2\pi}{15}\cos 4\theta+\ldots\right) \quad (15)$$

where γ ranges from -1 to 1; δ ranges from 0 to 1. Equation (15) is the standard class B power amplifier drain current expression.

The output power $P_{1,RRJ}$, DC power $P_{DC,RRJ}$, drain efficiency η_{RRJ} are derived from Equations (14) and (15) [19].

$$P_{1,RRJ} = \frac{(1-\delta)}{4}V_{DD}I_{\text{Max}} \quad (16)$$

$$P_{DC,RRJ} = \left(1-\frac{\delta}{2}\right)\frac{V_{DD}I_{\text{Max}}}{\pi} \quad (17)$$

$$\eta_{RRJ} = \frac{\pi(1-\delta)}{4-2\delta} * 100\% \quad (18)$$

Due to the addition of impedance factor, the value of the real part of the coefficient of DC voltage in Equation (14) by the δ is not zero, but in reality, the DC voltage is a constant value and does not change with the change of δ, which means that the ideal DC power is less than the actual situation, so the actual DC power is revised.

$$P_{DC,RRJ} = \frac{V_{DD}I_{\text{Max}}}{\pi} \quad (19)$$

Equation (19) is the modified DC power expression. The modified drain efficiency expression is then obtained by Equations (16) and (19):

$$\eta_{RRJ} = \frac{\pi}{4}(1-\delta) * 100\% \quad (20)$$

In order to make the drain efficiency in this mode greater than 60%, the value of δ ranges from 0 to 0.23.

The fundamental impedance as well as the second harmonic impedance of the resistive response class J power amplifier can be calculated from Equations (14) and (15):

$$Z_{1,RRJ} = R_{opt}\left((1-\delta)+j\gamma\left(1-\frac{\delta}{4}\right)\right) \quad (21)$$

$$Z_{2,RRJ} = \frac{3\pi}{8}R_{opt}(\delta-j\gamma(1-\delta)) \quad (22)$$

From the value range of δ when the drain efficiency is greater than 60%, combined with Equations (21) and (22), the corresponding impedance space can be drawn, as shown in Figure 2.

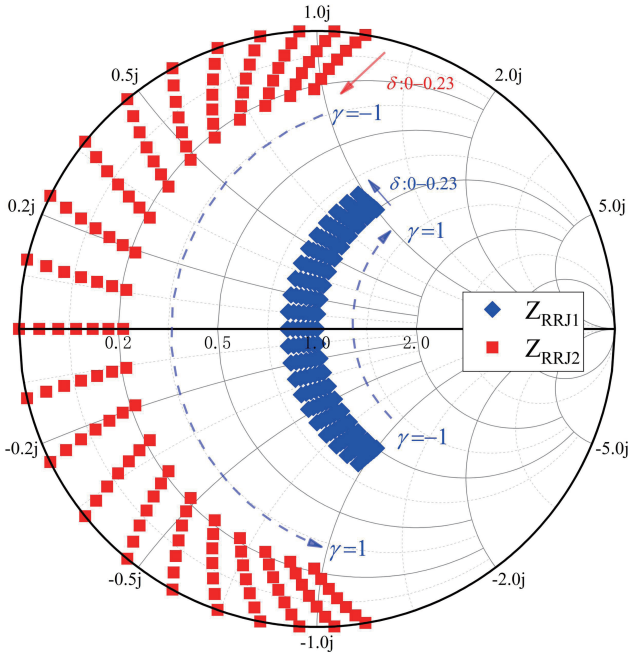

FIGURE 2. The impedance design space for resistive response class J amplifiers.

Similarly, the fundamental power $P_{1,RRF}$, drain efficiency η_{RRF}, fundamental impedance expression $Z_{1,RRF}$, second harmonic impedance expression $Z_{2,RRF}$, and third harmonic impedance expression $Z_{3,RRF}$ can be calculated from the resistive response class F power amplifier's voltage expression (23) and Equation (15) for this mode.

$$V_{DS,RRF}(\theta) = V_{DD}\left(1-\frac{2}{\sqrt{3}}\cos\theta+\frac{1}{3\sqrt{3}}\cos 3\theta\right)(1-\gamma\sin\theta)(1+\delta\cos\theta) \quad (23)$$

$$P_{1,RRF} = \frac{2-\sqrt{3}\delta}{4\sqrt{3}}V_{DD}I_{\text{Max}} \quad (24)$$

$$\eta_{RRF} = \frac{2-\sqrt{3}\delta}{4\sqrt{3}}\pi * 100\% \quad (25)$$

$$Z_{1,RRF} = R_{opt}\left(\left(\frac{2}{\sqrt{3}}-\delta\right)+j\gamma\left(1-\frac{7\delta}{12\sqrt{3}}\right)\right) \quad (26)$$

$$Z_{2,RRF} = \frac{3\pi}{8}R_{opt}\left(\frac{5\delta}{3\sqrt{3}}-j\gamma\left(\frac{7}{3\sqrt{3}}-\delta\right)\right) \quad (27)$$

$$Z_{3,RRF} = \infty \quad (28)$$

As with resistive response class J power amplifiers, the real part of the DC voltage in Equation (23) results in a theoretical drain efficiency that is greater than the actual situation, and Equation (25) corrects the drain efficiency expression [20].

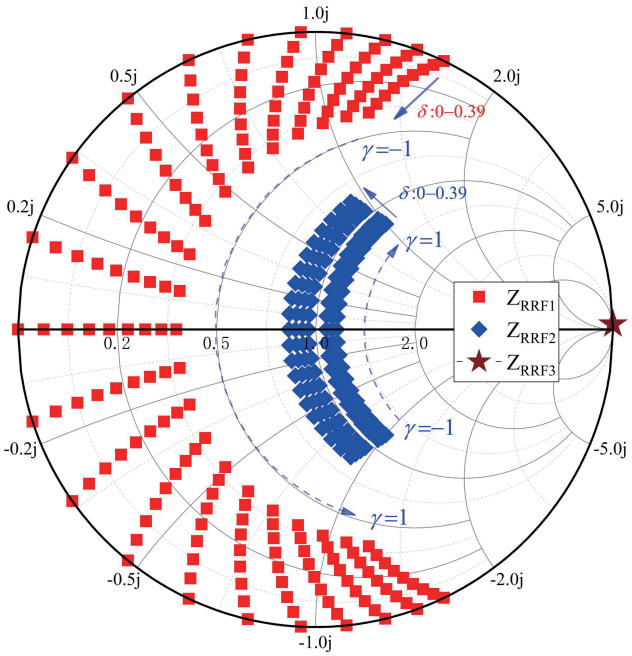

FIGURE 3. The resistive response class F amplifier impedance design space.

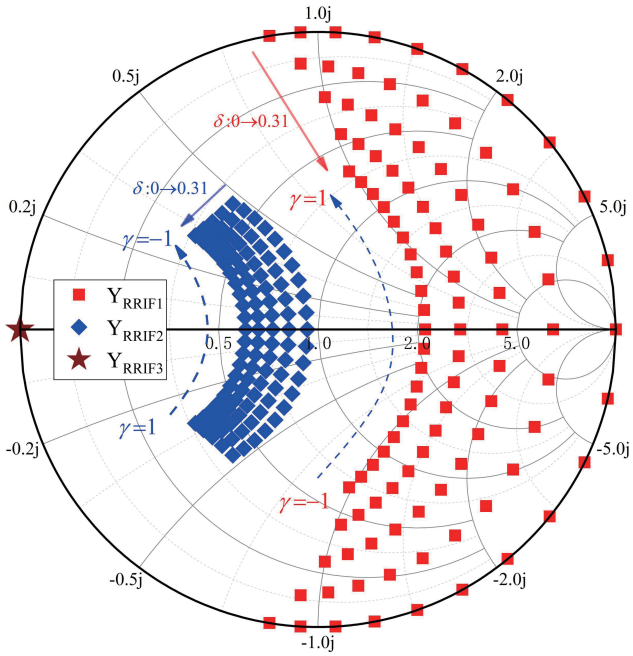

FIGURE 4. The resistive reactance inverse class F amplifier impedance design space.

The corresponding impedance design space is plotted by combining the range of values of δ [0, 0.39] for this mode with drain efficiency greater than 60%, as shown in Fig. 3.

In line with the resistive response class J amplifier, the drain efficiency and conductance expressions for the inverse class F amplifier, also featuring resistive response, are outlined below [21]:

$$\eta_{RRIF} = \frac{\sqrt{2}\,(1.16-\delta)}{2} * 100\% \tag{29}$$

$$Y_{1,RRIF} = \sqrt{2}G_{opt}\,(1.16-\delta) - j\gamma\,(0.33\delta - 1) \tag{30}$$

$$Y_{2,RRIF} = 2G_{opt}\,(\delta - j\gamma\,(1.32-\delta)) \tag{31}$$

$$Y_{3,RRIF} = \infty \tag{32}$$

The impedance design space corresponding to the range of values of δ in [0, 0.31] for drain efficiency greater than 60% is shown in Fig. 4.

Based on the three modes of power amplifiers proposed above, these three modes are combined and designed to realize the resistive response hybrid continuous class operation mode, which has a more flexible impedance space and a larger range of impedance variation than the traditional single-mode operation mode, and expands the bandwidth while ensuring the efficiency.

3. FILTER POWER AMPLIFIER DESIGN

Drawing upon the aforementioned theory, three distinct resistive reactance modes are devised by substituting the standard $\lambda/4$ transmission line with an interdigital bandpass filter. This substitution enables the control of harmonic impedance. The filter's capability to suppress out-of-band total reflection displays pure reactance features, modifying the voltage and current profiles of the harmonics at the circuit's drain. Consequently, it generates a precise voltage-current waveform [22–24], positioning the circuit's high harmonic impedance on the Smith chart's periphery, thereby achieving a highly efficient broadband power amplifier.

GaN CG2H40010F transistor from Cree is used in this paper. According to the metrics designed in this paper on the basis of the eighth order Chebyshev low-pass filter [25–27], the low-pass model is converted into a band-pass model by the low-pass-to-conductance frequency transformation Equations (33)–(35), and its overall circuit is shown in Fig. 5. The input consists of a matching circuit and a biasing circuit with an RC stabilizing network as well as an isolation capacitor, which is used to ensure the stability of the amplifier and to block DC. The output consists of a bias circuit and an interdigital bandpass filter connected to the transistor through two sections of microstrip lines, which act as an impedance transformer to solve the impedance mismatch between the transistor and the filter, and serve as a soldering plate to facilitate the physical processing of soldering.

$$\omega' = \frac{\omega_1'}{FBW}\left(\frac{\omega}{\omega_0} - \frac{\omega_0}{\omega}\right) \tag{33}$$

$$FBW = \frac{\omega_2 - \omega_1}{\omega_0} \tag{34}$$

$$\omega_0 = \sqrt{\omega_1\omega_2} \tag{35}$$

In order to achieve broadband high efficiency, the transistor drain terminal impedance is controlled to the range corresponding to each mode, and there is an overlap of the impedance conditions corresponding to each mode, which in turn realizes the mode combination [28, 29]. The harmonic impedance

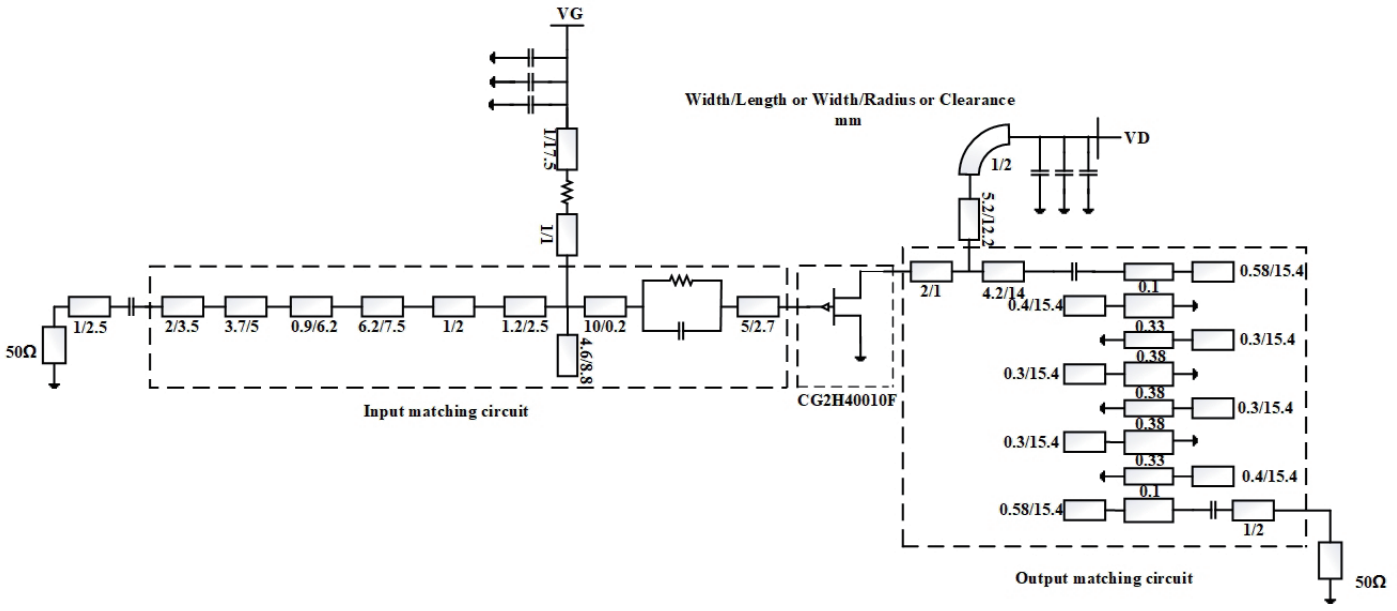

FIGURE 5. Overall circuit dimensions of the power amplifier.

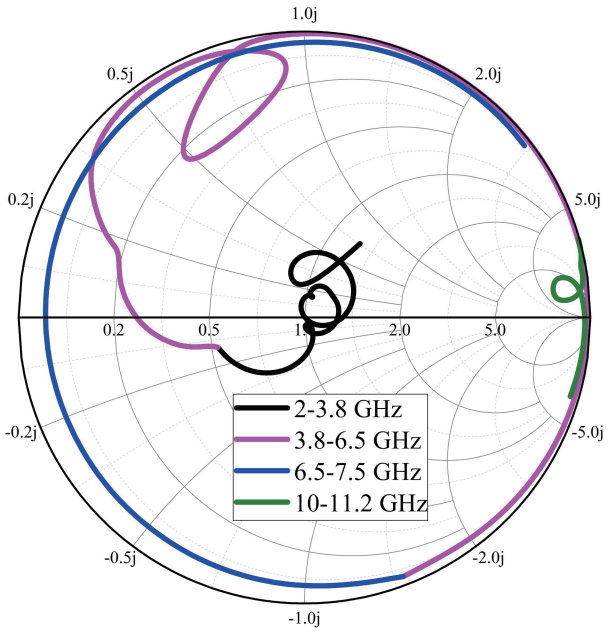

FIGURE 6. Impedance traces at the drain end of the amplifier.

simulation results are shown in Fig. 6, which shows that the circuit impedance trajectory matches the impedance space of the corresponding mode. Some frequency bands correspond to impedance trajectories that deviate from the impedance design space, and it has been demonstrated by many researchers that high efficiencies can still be maintained in most regions outside the impedance design space of resistive response power amplifiers.

4. IMPLEMENTATION AND MEASUREMENT

The proposed power amplifier was simulated using Advanced Design System (ADS) and processed for testing. Rogers 4003C ($H = 0.813$, $\varepsilon = 3.38$) and GaN HEMT transistor CG2H40010F were used to design and fabricate the power amplifier operating at 2–3.8 GHz with a gate bias voltage of -2.7 V and a drain bias voltage of 28 V. The dimensional drawing of the power amplifier is shown in Fig. 5. The physical processing diagram of the power amplifier is shown in Fig. 7.

The power amplifier functioned under continuous wave signals ranging from 2 to 3.8 GHz, yielding a saturated output power within 39.1 to 41.2 dBm. Across this frequency band, the drain efficiency (DE) varied from 56.3% to 75.5%, and the gain ranged from 11.1 to 13.2 dB, as depicted in Fig. 8. It can be seen from Fig. 6 that the impedance trajectory near 3 GHz does not fall in the impedance space, and the impedance trajectory rotates clockwise along the Smith circle diagram. As the frequency approaches 3 GHz, the efficiency decreases somewhat, but still maintains a high efficiency. Additionally, Fig. 9 illustrates the trends of gain and DE against input power, revealing a marked decline in gain beyond 30 dB input power, while DE approaches saturation. Fig. 10 shows the change curve of gain and DE with the output power. It can be seen that the gain decreases significantly when the output power is large and 40 dB, and the efficiency is close to saturation.

The current-voltage waveforms at 2.25 GHz, 2.6 GHz, and 3.65 GHz are given below. Fig. 11(a) displays the current-voltage profiles at the drain of the power amplifier functioning at 2.25 GHz, revealing a current waveform resembling a square wave and a voltage waveform akin to a sine wave, indicating operation in the resistive response inverse class F mode. In Fig. 11(b), the current and voltage waveforms at 2.6 GHz show both similar to sine waves, suggesting that the amplifier operates in the resistive response class J mode. Meanwhile, Fig. 11(c) depicts the waveforms at 3.65 GHz, where the current waveform mimics a sine wave while the voltage waveform resembles a square wave, indicating operation in the resistive response class F mode.

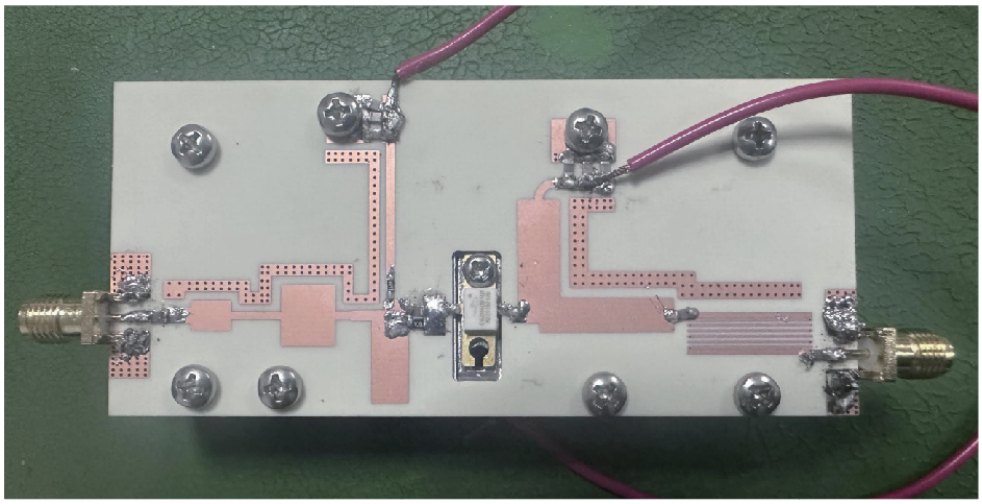

FIGURE 7. Physical photographs of the power waiver produced.

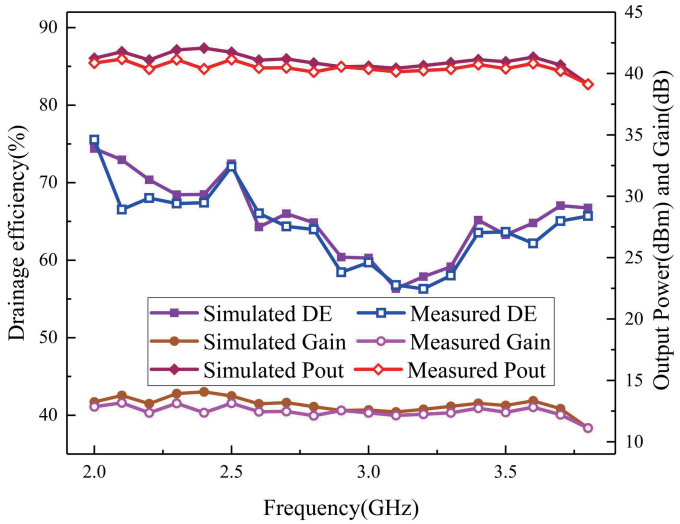

FIGURE 8. The simulated and measured DE and gain under the saturated output power.

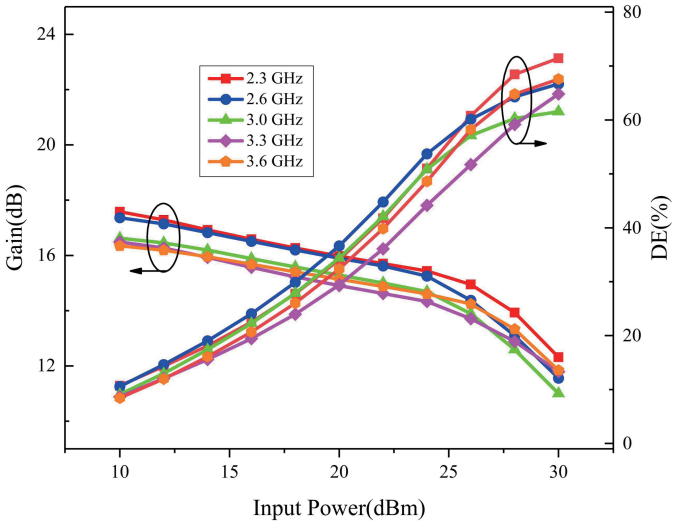

FIGURE 9. The measured gain and DE versus input power.

TABLE 1. Comparison with other referenced power amplifiers.

Reference	Bandwidth	Efficiency (%)	Output power (dBm)	Gain (dB)
[2]	0.8–3	55–68.5	39.8–42.4	8.5–14.2
[7]	2.95–3.35	51–67	40	10
[8]	2–3.8 GHz	47–60	40.6–41.7	13.4–15.1
[10]	0.5–1.8 GHz	50–69	39–40.8	-
	1.6–2.2 GHz	55–68	40–41	-
[25]	3.3–3.6 GHz	62.3–68.9	40.4–40.6	10.9–11.4
This work	2–3.8 GHz	56.3–75.5	39.1–41.2	11.1–13.2

Table 1 shows the performance comparison of the designed power amplifier with some published articles. Although the bandwidth and output power of [2] are better than that of this work, the efficiency and gain flatness of this work are better than that of [2]. Considering the efficiency, output power, gain, and other indicators, it can be seen that the power amplifier designed in this paper performs better than other power amplifiers and can be better used in practical applications.

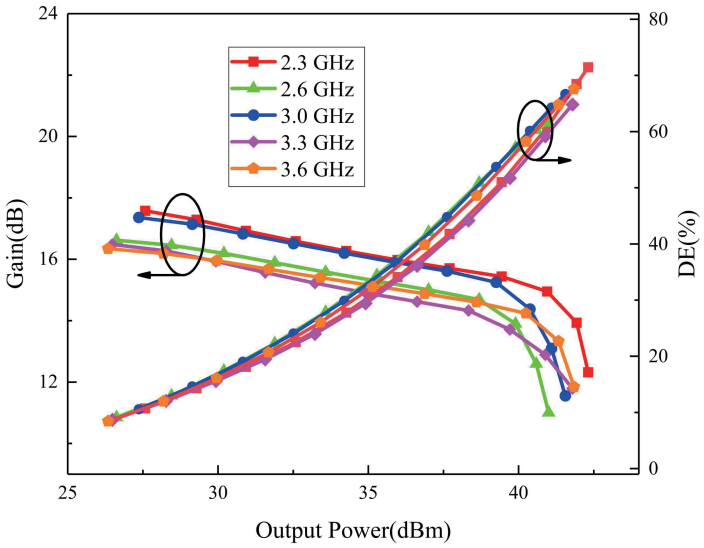

FIGURE 10. The measured gain and DE versus output power.

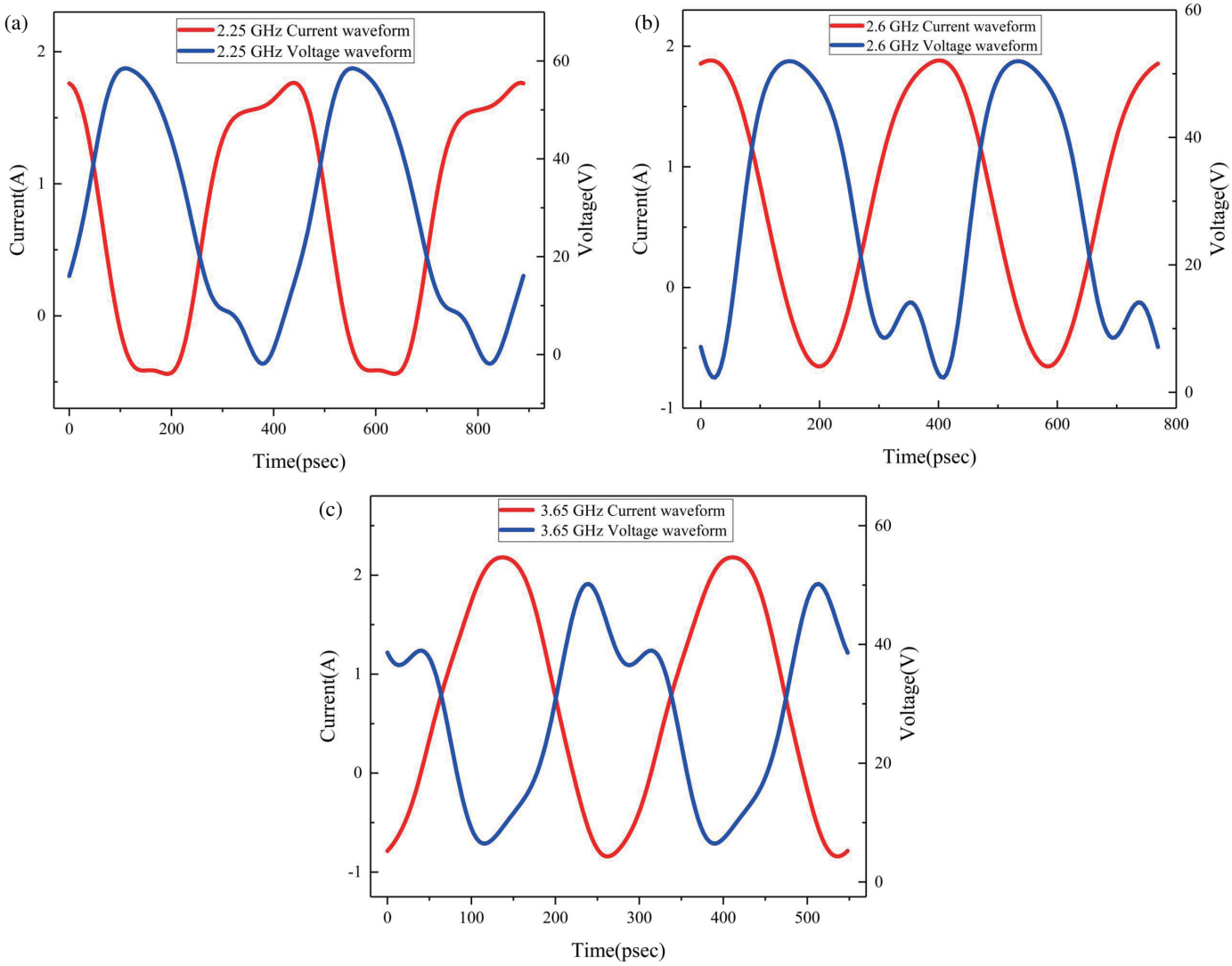

FIGURE 11. Voltage and current waveforms.

5. CONCLUSION

This paper presents the design of a multimode hybrid power amplifier incorporating an interdigital band-pass filter. Instead of the traditional $\lambda/4$ harmonic control network, the filter is employed to manage harmonic impedance, while the amalgamation of the multimode hybrid and continuous class operating modes offers enhanced design flexibility for achieving a broadband, high-efficiency amplifier. Subsequently, power amplifiers were constructed and tested across the 2 to 3.8 GHz range, yielding measured drain efficiency (DE) values between 56.3% and 75.5%, output power ranging from 39.1 to 41.2 dBm, and gain spanning 1.1 to 13.2 dB.

ACKNOWLEDGEMENT

This paper is supported by the Major Special Project for Technological Innovation and Application Development in Chongqing (CSTB2023TIAD-STX00I7) and also by Chengdu Regional Science and Technology Innovation Cooperation Project (2023-YF11-00046-HZ).

REFERENCES

[1] Shi, W., S. He, W. Shi, C. Shen, C. Li, Z. Xiao, and F. You, "Design of a C-band high efficiency power amplifier with compact harmonic control network," *IEEE Microwave and Wireless Components Letters*, Vol. 31, No. 9, 1059–1062, 2021.

[2] Li, C., F. You, T. Yao, J. Wang, W. Shi, J. Peng, and S. He, "Simulated annealing particle swarm optimization for high-efficiency power amplifier design," *IEEE Transactions on Microwave Theory and Techniques*, Vol. 69, No. 5, 2494–2505, 2021.

[3] You, F. and J. Benedikt, "An optimized-load-impedance calculation and mining method based on I–V curves: Using broadband class-E power amplifier as example," *IEEE Transactions on Industrial Electronics*, Vol. 66, No. 7, 5254–5263, 2018.

[4] Chen, K., J. Lee, W. J. Chappell, and D. Peroulis, "Co-design of highly efficient power amplifier and high-Q output bandpass filter," *IEEE Transactions on Microwave Theory and Techniques*, Vol. 61, No. 11, 3940–3950, 2013.

[5] Guo, Q.-Y., X. Y. Zhang, J.-X. Xu, Y. C. Li, and Q. Xue, "Bandpass class-F power amplifier based on multifunction hybrid cavity–microstrip filter," *IEEE Transactions on Circuits and Systems II: Express Briefs*, Vol. 64, No. 7, 742–746, 2016.

[6] Moon, J., S. Jee, J. Kim, J. Kim, and B. Kim, "Behaviors of class-F and class-F−1 amplifiers," *IEEE Transactions on Microwave Theory and Techniques*, Vol. 60, No. 6, 1937–1951, 2012.

[7] Chen, K., T.-C. Lee, and D. Peroulis, "Co-design of multiband high-efficiency power amplifier and three-pole high-Q tunable filter," *IEEE Microwave and Wireless Components Letters*, Vol. 23, No. 12, 647–649, 2013.

[8] Wang, W., H. Zhao, Y. Wu, and X. Chen, "5G wideband bandpass filtering power amplifiers based on a bandwidth-extended bandpass matching network," *China Communications*, Vol. 20, No. 11, 56–66, 2023.

[9] Woo, Y. Y., Y. Yang, and B. Kim, "Analysis and experiments for high-efficiency class-F and inverse class-F power amplifiers," *IEEE Transactions on Microwave Theory and Techniques*, Vol. 54, No. 5, 1969–1974, 2006.

[10] Mimis, K., K. A. Morris, S. Bensmida, and J. P. McGeehan, "Multichannel and wideband power amplifier design methodology for 4G communication systems based on hybrid class-J operation," *IEEE Transactions on Microwave Theory and Techniques*, Vol. 60, No. 8, 2562–2570, 2012.

[11] Wang, J., S. He, F. You, W. Shi, J. Peng, and C. Li, "Codesign of high-efficiency power amplifier and ring-resonator filter based on a series of continuous modes and even-odd-mode analysis," *IEEE Transactions on Microwave Theory and Techniques*, Vol. 66, No. 6, 2867–2878, 2018.

[12] Cripps, S. C., P. J. Tasker, A. L. Clarke, J. Lees, and J. Benedikt, "On the continuity of high efficiency modes in linear RF power amplifiers," *IEEE Microwave and Wireless Components Letters*, Vol. 19, No. 10, 665–667, 2009.

[13] Huang, C., S. He, W. Shi, and B. Song, "Design of broadband high-efficiency power amplifiers based on the hybrid continuous modes with phase shift parameter," *IEEE Microwave and Wireless Components Letters*, Vol. 28, No. 2, 159–161, 2018.

[14] Wang, Q., J. Nan, and R. Liu, "Design of high efficiency microstrip bandpass filtering power amplifier," in *2023 3rd International Conference on Electronic Information Engineering and Computer Science (EIECS)*, 1136–1140, Changchun, China, Sep. 2023.

[15] Xu, J., N. Yu, B. Shi, and Q. Zhao, "The miniaturization design of microstrip interdigital bandpass filter," in *2009 2nd International Conference on Power Electronics and Intelligent Transportation System (PEITS)*, Vol. 3, 74–76, Shenzhen, China, Dec. 2009.

[16] Wong, J. S., "Microstrip tapped-line filter design," *IEEE Transactions on Microwave Theory and Techniques*, Vol. 27, No. 1, 44–50, 1979.

[17] Hong, J.-S. G. and M. J. Lancaster, *Microstrip Filters for RF/Microwave Applications*, John Wiley & Sons, 2004.

[18] Carrubba, V., M. Akmal, R. Quay, J. Lees, J. Benedikt, S. C. Cripps, and P. J. Tasker, "The continuous inverse class-F mode with resistive second-harmonic impedance," *IEEE Transactions on Microwave Theory and Techniques*, Vol. 60, No. 6, 1928–1936, 2012.

[19] Friesicke, C., R. Quay, and A. F. Jacob, "The resistive response class-J power amplifier mode," *IEEE Microwave and Wireless Components Letters*, Vol. 25, No. 10, 666–668, 2015.

[20] Zheng, S. Y., Z. W. Liu, X. Y. Zhang, X. Y. Zhou, and W. S. Chan, "Design of ultrawideband high-efficiency extended continuous class-F power amplifier," *IEEE Transactions on Industrial Electronics*, Vol. 65, No. 6, 4661–4669, 2017.

[21] Tang, Q.-H., Y.-H. Li, and W.-G. Li, "Over second octave power amplifier design based on resistive-resistive series of continuous class-F/F−1 modes," *IEEE Microwave and Wireless Components Letters*, Vol. 27, No. 5, 494–496, 2017.

[22] Grebennikov, A., "High-efficiency class-E power amplifier with shunt capacitance and shunt filter," *IEEE Transactions on Circuits and Systems I: Regular Papers*, Vol. 63, No. 1, 12–22, 2016.

[23] Wright, P., J. Lees, J. Benedikt, P. J. Tasker, and S. C. Cripps, "A methodology for realizing high efficiency class-J in a linear and broadband PA," *IEEE Transactions on Microwave Theory and Techniques*, Vol. 57, No. 12, 3196–3204, 2009.

[24] Du, X., C. J. You, J. Cai, M. Helaoui, F. M. Ghannouchi, Y. Zhao, and X. Li, "Novel design space of load modulated continuous class-B/J power amplifier," *IEEE Microwave and Wireless Components Letters*, Vol. 28, No. 2, 156–158, 2018.

[25] Zhuang, Z., Y. Wu, M. Kong, and W. Wang, "High-selectivity single-ended/balanced DC-block filtering impedance transformer and its application on power amplifier," *IEEE Transactions on Circuits and Systems I: Regular Papers*, Vol. 67, No. 12, 4360–4369, 2020.

[26] Zhou, L.-H., X. Y. Zhou, W. S. Chan, T. Sharma, and D. Ho, "Wideband class-F−1 power amplifier with dual-/quad-mode

bandpass response," *IEEE Transactions on Circuits and Systems I: Regular Papers*, Vol. 67, No. 7, 2239–2249, 2020.

[27] Li, Y. C., K. C. Wu, and Q. Xue, "Power amplifier integrated with bandpass filter for long term evolution application," *IEEE Microwave and Wireless Components Letters*, Vol. 23, No. 8, 424–426, 2013.

[28] Xuan, X., F. Yang, and C. Liu, "Design of multioctave high-efficiency power amplifier based on extended continuous Class-B/J modes," *International Journal of RF and Microwave Computer-Aided Engineering*, Vol. 29, No. 10, e21899, 2019.

[29] Chen, J., S. He, F. You, R. Tong, and R. Peng, "Design of broadband high-efficiency power amplifiers based on a series of continuous modes," *IEEE Microwave and Wireless Components Letters*, Vol. 24, No. 9, 631–633, 2014.